

# Multi-objective Optimal Design for Carrier and Torque Frame Assembled Together in Planetary Gear Train of GTF by Integrated DOE, RSM and LSGRG

Chao Liu \* and Zong-De Fang \*\*

**Keywords :** multi-objective structural optimization, parameterized finite element model, planetary gear transmission system, geared turbo fan, design of experiment, response surface method.

## ABSTRACT

An approach of multi-objective optimal design for carrier and torque frame assembled together in planetary gear system of Geared Turbo Fan (GTF) is proposed in this paper. First, a program package is developed as parameterized model in Python language, the main function of which is to achieve automatic invoking of complete FEA during optimization. Therefore, development cycle of the product is reduced greatly. Second, significant factors are selected based on design of experiment (DOE) respectively for maximum von Mises stress of the frame and maximum displacement of the holes on the carrier. Third, sampling values of the two responses are obtained by central composite face-centered (CCF) design. Next, approximate quadratic polynomials are found through response surface method (RSM) to express the two objective functions explicitly. Finally, the Pareto efficient solution of three optimization objectives (total mass and the two) is acquired via large scale generalized reduced gradient (LSGRG) algorithm. The simulation results show that the relative error of each response is less than 5%, which indicates that the model proposed is quite correct. Furthermore, the comparison also reveals that the approach integrated DOE, RSM and LSGRG to determine the most favorable configuration of the assembly is appropriate and effective.

*Paper Received October, 2016. Revised December, 2016. Accepted February, 2017. Author for Correspondence: Fang Zong-De.*

\* *Doctoral Student, School of Mechanical Engineering, Northwestern Polytechnical University, Xi'an, China, 710072.*

\*\* *Professor, doctoral supervisor, School of Mechanical Engineering, Northwestern Polytechnical University, Xi'an, China, 710072. E-mail address: fauto@nwpu.edu.cn.*

## INTRODUCTION

Compared with traditional engine, Geared Turbo Fan (GTF) has the characteristics of higher thrust and larger bypass ratio. Besides, it has many advantages such as lower noise, less fuel consumption and maintenance costs. Hence, it is considered widely to be main choice of new generation civil engine. There will be 38,050 new airplanes needed. Most importantly, 26,730 of them (about 70 percent) will be single-aisle from 2015 to 2034 (Company Boeing, 2014). As new impetus of the next generation of single-aisle airplanes, GTF has attracted more and more attention.

The main superiority of GTF against ordinary turbofan engine is its planetary gear transmission system assembled. Therefore, design of the gear reducer has been the key to success among many core technologies. Because power offered by GTF is much higher than the one by current engine, there are many higher design requirements to be met. First, due to increased diameters of the reducer, the whole mass of GTF increases greatly. In spite of those advantages, GTF may be hardly applied in the future if the mass problem cannot be settled properly. Furthermore, mechanical properties of GTF determine many basic design parameters of the reducer. Consequently, how to decrease mass of gearbox has become a top priority. Second, stiffness and strength check also needs considering during development of the product.

Generally, mathematic model of optimal problem is known before solved. In other words, objective functions and constraint conditions are determined as explicit formulas by analytic method (Zhan et al., 2013; Ashjari et al., 2014; Kuzmin et al., 2014). For example, mass of the gearbox can be expressed explicitly as objective function to optimize. Nevertheless, most of these cases are suitable for simple structures usually. Zhou et al. (2013) proposed a generic method to design engineering features for level set based structural optimization, and the authors believe that the features are regular and

simple shape units containing specific engineering significance. Losanno et al. (2015) conducted an optimal design procedure for a simple frame equipped with elastic-deformable dissipative braces. However, for complicated structures even an entire mechanical system, relationship between design variables and optimal objectives are uncertain, or it is difficult to build the explicit expression as objective function for optimization (Si et al., 2014; Hansen et al., 2008; Shin et al., 2015).

During the optimization of stiffness and strength of gearbox, one big challenge is that the explicit formulas between the design variables and the two responses are scarcely expressed. The other crucial problem is that it will consume large computing hardware resources and lots of time to calculate displacement and stress as responses. This is because most of optimization algorithms need vast iterations to assure the convergence precision. In addition, the algorithms need to invoke finite element analysis (FEA) to determine solutions during iterations. Thus, for such a complicated system, it may cost several days even weeks to obtain the final optimal result after thousands of iterations. To solve the two problems above, design of experiment (DOE) and response surface methodology (RSM) are better choices.

DOE is of fundamental importance in engineering design activities, and it is a critically important tool in the scientific and engineering world for improving the product realization process (Fattahi, et al., 2014; Relkar, et al., 2012; Gurralla, et al., 2014). Some objectives and applications of DOE include (Montgomery, 2012): (1) selection of parameters to guarantee favorable product; (2) determining which variables are most influential on response; (3) determining values of variables to make sure that the corresponding response reaches a maximum or minimum value, or is almost near a desired nominal value; (4) reducing development time and costs.

RSM is a collection of mathematical and statistical techniques useful for modeling and analysis of the problems in which a response of interest is influenced by several variables and the objective is to optimize this response (Montgomery, 2012). In most RSM problems, the form of relationship between responses (such as stiffness and strength of the gearbox) and independent input variables is unknown. Eventual purpose of RSM is to determine the optimum operating conditions for the system or to determine a region of the factor space in which operating requirements are satisfied (Anderson-Cook et al., 2009; Wang et al., 2013; Sharma et al., 2014).

Focusing on the structural optimization design for the assembly of carrier and torque frame in GTF, this paper is to combine DOE, RSM and Large Scale Generalized Reduced Gradient (LSGRG) algorithm to determine the best values of design variables in order that total mass of the system can be minimized

with sufficient strength and proper stiffness. First, the parameterized finite element (FE) model of the planetary gear transmission system needs building by Python Language on ABAQUS re-development platform so that the FE model can be modified and updated automatically when LSGRG adjusts values of the design variables and invokes the computational process of FEA. Second, insignificant factors are to be eliminated, and influential variables are to be selected as design variables according to DOE. Third, with central composite face-centered design (CCF) used as sampling method, two response surface models need to be found respectively for strength and stiffness as objective functions based on RSM approximating technique. Finally, optimum values of the design parameters will be determined through LSGRG, and the best geometrical configuration of the assembly will be determined.

The priorities of the paper are as follows. First, with full automation, the whole optimization process is carried out by the integrated programs. Second, computing hardware resources and development cycle are reduced extremely because of the python script program and the sampling numbers of DOE and CCF. Third, explicit formulas are found for the relationship between the four optimization variables and two responses. Finally, the optimal structure of the assembly is determined.

## AUTOMATIC PARAMETERIZED FE MODEL OF THE SYSTEM

Different from ordinary gas turbine, there is one gear reducer assembled in GTF between a fan and low-pressure compressor of a two-stage turbofan system. This allows the fan, compressor and turbine to work under their most effective working conditions respectively so that GTF engine achieves the best synthetical performance. Figure 1 (Sheridan, 2013) shows typical structure of the engine.

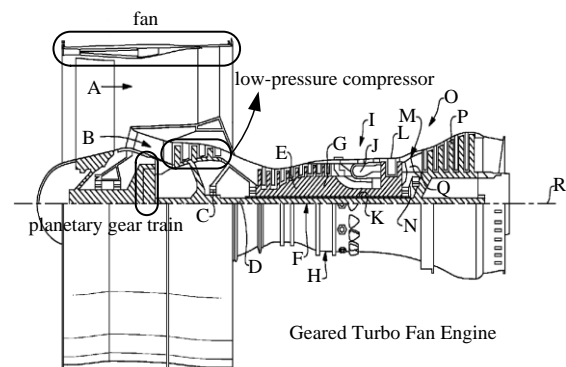


Fig.1 A partial cross-sectional view of a front portion of GTF: A, bypass flow path; B, core flowpath; C, bearing systems; D, inner shaft; E, high-pressure compressor; F, low-speed spool; G, high-speed spool; H, engine static

structure; I, combustor section; J, combustor; K, outer shaft; L, high-pressure turbine; M, mid-turbine frame; N, bearing systems; O, turbine; P, low-pressure turbine; Q, airfoil; R, engine central longitudinal axis.

Generally, a planetary gear train connected to a turbine section of the engine is employed as a gear reducer. It consists of four parts (McCune et al., 2014): a sun gear driven by low-pressure turbine; a ring gear connected with the fan; five intermediate gears meshed with the sun gear and ring gear simultaneously; a unitary carrier having bolted connection with a torque frame fixed to the engine static structure for improving strength and rigidity. Fig.2 (Sheridan, 2012) shows typical structure of the planetary gear train. In fact, it is an epicyclical transmission system with herringbone gears. The system receives rotational input from input shaft in practice, one end of which is connected with a compressor shaft, and the other is connected with a sun gear by spline connection. Five intermediate gears supported by a unitary carrier surrounds and meshes with the sun gear inwardly, and a ring gear surrounds and meshes with the intermediate gears outwardly. The carrier is fixed to the housing of the system against rotation. Thus, the intermediate gears are referred to as “star” gears, and the ring gear is secured to the output shaft that supports the turbo fan.

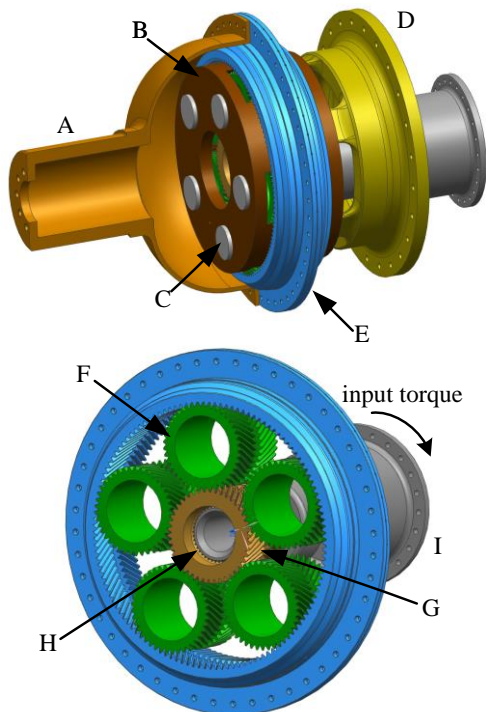
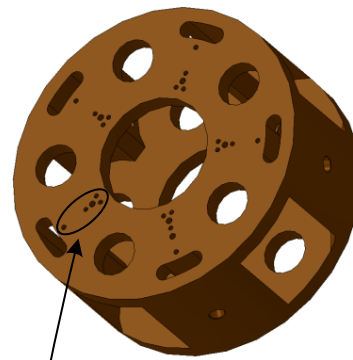
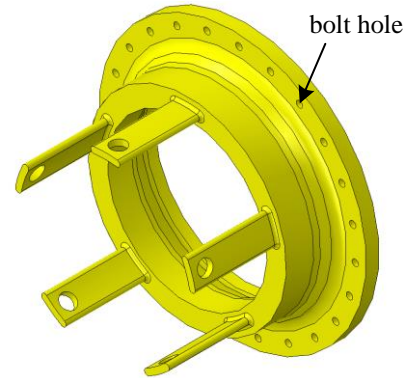
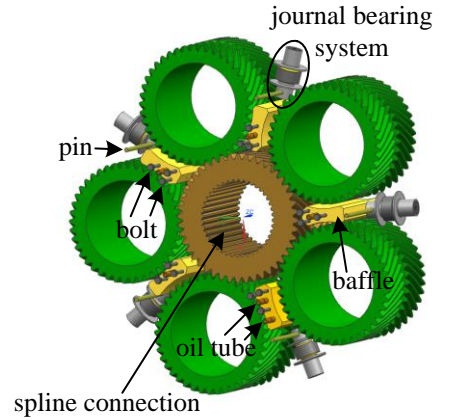


Fig.2 typical structure of epicyclical transmission system: A, output shaft; B, carrier; C, bearing system; D, torque frame; E, ring gears; F, intermediate gear; G, sun gear; H, splined connection; I, input shaft.

### Proper treatment to simplify the system for FEA

Because one of the main purposes of this paper is to reduce calculation consumption during FEA of the system for optimizing the carrier assembled with the frame, some proper treatments to simplify the system are accomplished as follows.



small holes receiving pins, bolts and oil tube

Fig.3 secondary features of the system in FEA for optimization aim.

First, some secondary features such as spline connection, pins, bolts, oil tubes, baffles, journal bearing systems and small holes shown in Fig.3 are without consideration because of their little contribution to the main purpose. Oppositely, these features may increase the scale of the FE model overly, and even cause calculation failure due to the distortion of FE mesh. Second, to simplify the FE

model, input shaft is replaced by a lumped mass point locating on geometric center of sun gear as shown in Fig.4 (a).

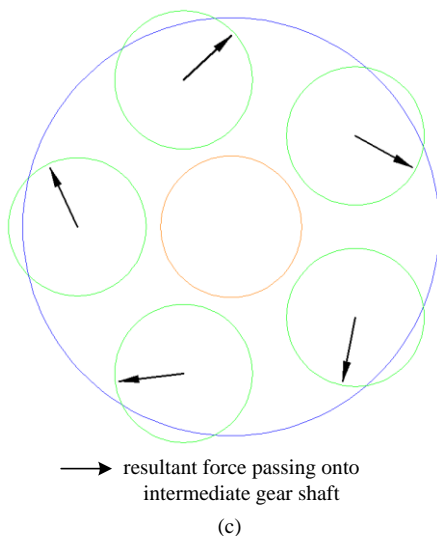
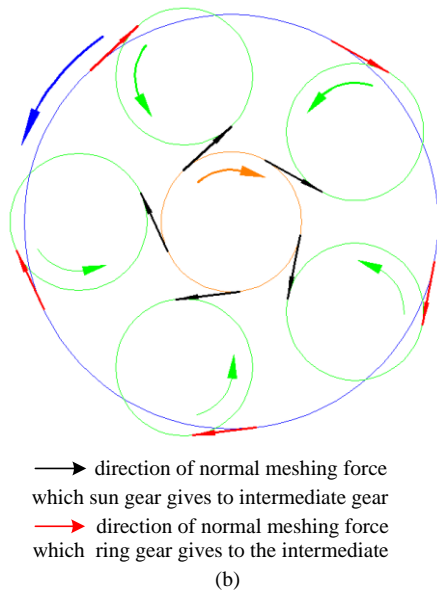
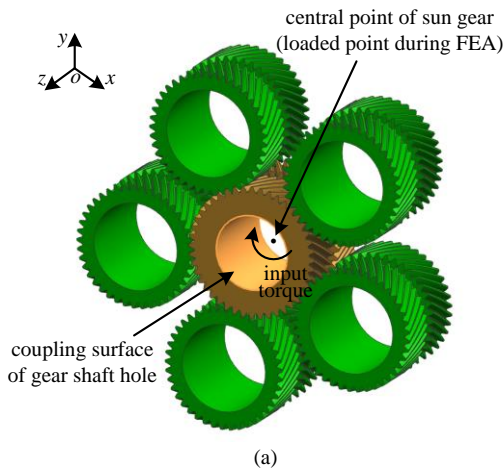
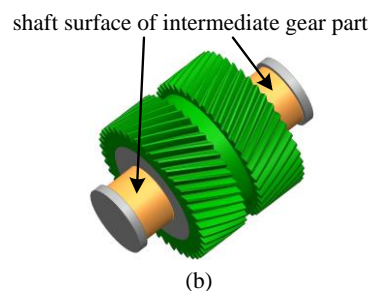
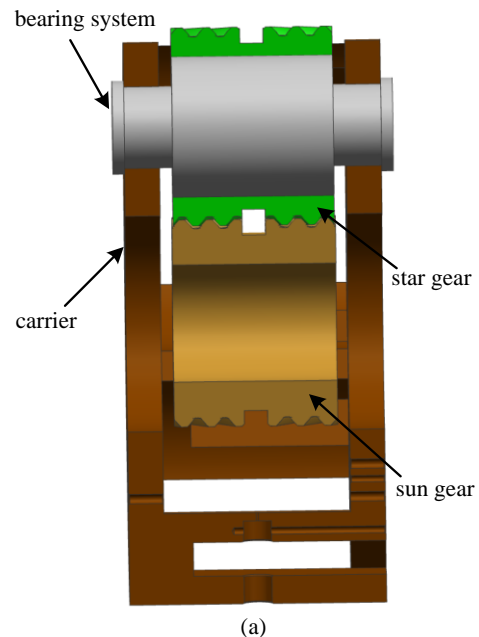


Fig.4 general process of force transfer inside the system.

Second, during FEA process, driving torque is loaded along z-axis upon the central point, which couples with the surface of shaft hole on sun gear shown in Fig.4 (a). Point-to-surface coupling method provided by ABAQUS is applied to deal with kinematic relationship between the point and sun gear. In this way, the input torque drives sun gear to move. Each of five intermediate gears is engaged with sun gear by teeth interfaces. Thus, when sun gear rotates, there exist normal meshing forces between gears as shown in Fig.4 (b). Next, the normal meshing force acting on intermediate gear (one is the force that sun gear gives, and the other is the force that ring gear gives) equals to a resultant force passing onto intermediate gear shaft shown in Fig.4 (c).

Third, intermediate gear connected with shaft by flat key is supported by roller bearing system that is fixed to the carrier as shown in Fig.5 (a). To simplify the modeling process, intermediate gear, flat key, gear shaft and rolling bearing are regarded as a whole part shown in Fig.5 (b) to avoid excessive contact pairs in multi-body FEA. According to definition of contact pair by ABAQUS, the gear shaft surface as shown in Fig.5 (b) connects with the surface of the hole on carrier shown in Fig.5 (c). Accordingly, the effect of five resultant forces passing onto the carrier equals to the effect of new torque acting on the carrier directly.



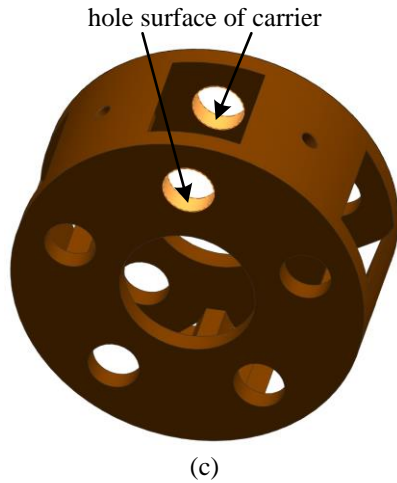


Fig.5 carrier subsystem (a) and intermediate gear part (b) contacting with carrier (c).

Fourth, the carrier has apertures shown in Fig.6 (a) to receive z-axially extending fingers of the frame. With pins, spherical bearings, bushings and fasteners, the carrier is grounded to the frame that is fixed to housing by circular-distribution bolts. In this way, force transmits from sun gear to intermediate gear and then to the carrier and eventually reaches the frame. Because the back surface of torque frame shown in Fig.6 (b) is fixed completely, the system finally reaches equilibrium under loading conditions.

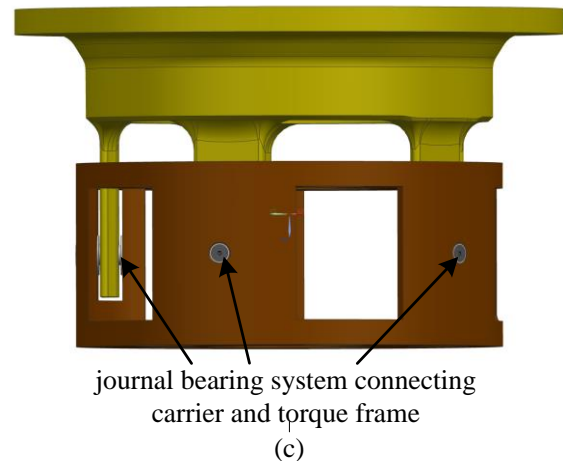
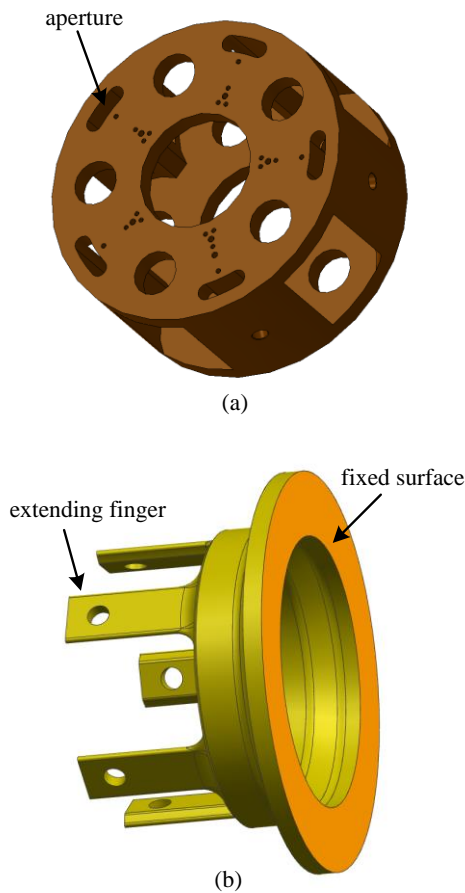


Fig. 6 aperture on carrier (a), fixed surface of torque frame (b) and the assembly with bearing(c).

During FE modeling process, journal bearing system is simplified as connector element provided by ABAQUS to connect fingers and carrier. Through constraining the corresponding degrees of freedom, relative motion relationship between the carrier and frame is determined. Fig.6 (c) (Sheridan, 2014) shows the assembly of carrier and frame.

Finally, output shaft as secondary components for optimal design are still without modeling in FEA. There are three ways adopted in the paper to mesh the system during FE modeling. (1) "Structured mesh generation technology" is used for basic geometry instance such as gear shaft, etc. (2) "local mesh densification technology" is applied in critical field such as contact area, chamfer and round of the finger on the frame, etc. (3) "free meshing technique" is used for irregular structure and the field that has less effect on results. Considering both computation accuracy and efficiency, careful decision was made on meshing strategy to guarantee high quality of FE model for each analysis. The eventual FE assembly of the planetary gear train in GTF is simplified as shown in Fig.7.

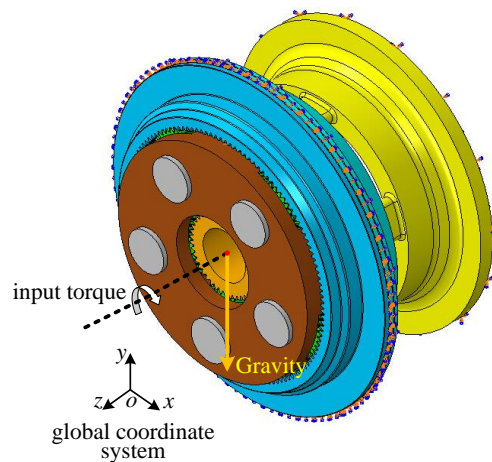


Fig. 7 FE model of the planetary gear train.

**Influential factors**

Due to the relationship between components of the assembly, basic geometric size has been determined previously. According to engineering experience, there are six input variables determined as influential factors ( $V_1$  to  $V_6$ ) shown in Fig.8.

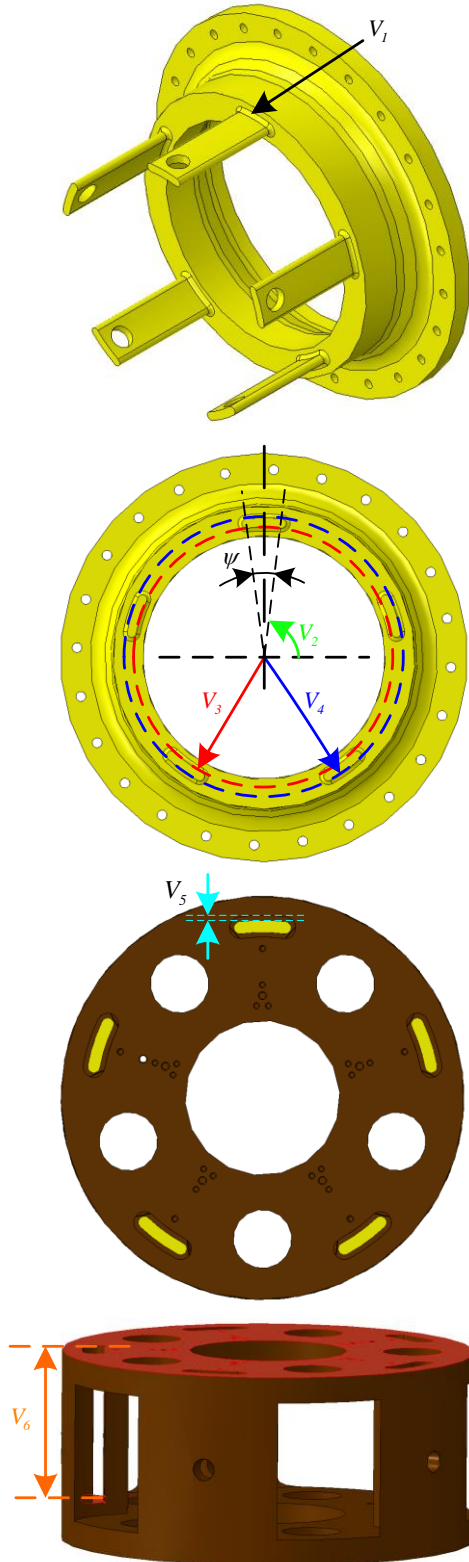


Fig.8 six input variables of the system.

The relationship between  $V_2$ ,  $V_3$ ,  $V_4$  and  $V_5$  is shown in Fig.9 particularly, and written as

$$\begin{cases} V_2 = \alpha = 90 - \frac{\psi}{2} \\ V_3 = R_1 \\ V_4 = R_2 \\ V_5 = R_1 - R_3 = R_4 - R_2 = r_2 - r_1 = r_4 - r_3 \end{cases}, \quad (1)$$

where  $r_1 = r_3 = \frac{1}{2}(R_2 - R_1)$ .

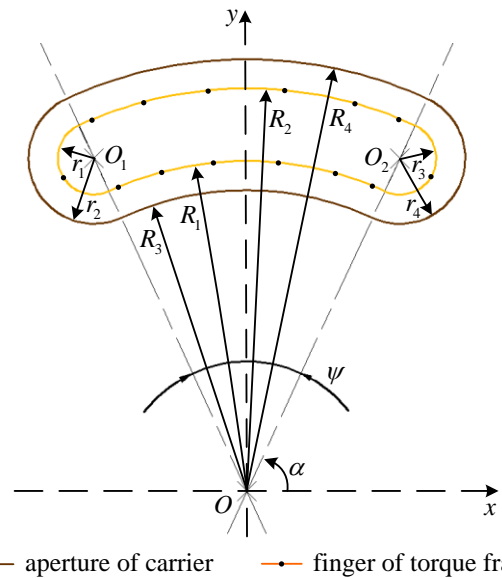


Fig.9 input variables ( $V_2$  to  $V_5$ ) in cross-sectional view of the finger assembled with carrier.

One finger on the frame is determined when the four variables have their own value. Further, the other four fingers on the frame are built through circular array based on the first one. At the same time, apertures on the carrier are built correspondingly.

**Output responses**

There are three output responses of the system to be optimized.

First, total mass of the system is expected to be minimal, which is expressed as

$$M_{total} = M_{carrier} + M_{torframe} + M_{gears}. \quad (2)$$

According to Appendix I,  $M_{total}$  is determined in detail as

$$M_{total} = 0.3256 - 5 \cdot \rho \cdot \pi \cdot \left\{ V_6 \cdot \left[ r_2^2 + \frac{R_4^2}{180} \cdot (90 - \alpha) - \frac{R_3^2}{180} \cdot (90 - \alpha) \right] - 190 \cdot \left[ r_1^2 + \frac{R_2^2}{180} \cdot (90 - \alpha) - \frac{R_1^2}{180} \cdot (90 - \alpha) \right] \right\} \quad (3)$$

Meanwhile, flexible design for input shaft guarantees equal load property of the system, which requires the assembly of carrier and frame to have enough stiffness and proper strength. To meet the requirements more conveniently during FEA, maximum displacement of the bearing holes shown in Fig.10 and maximum von Mises equivalent stress of the frame are expected as the other two output responses to be minimized simultaneously.

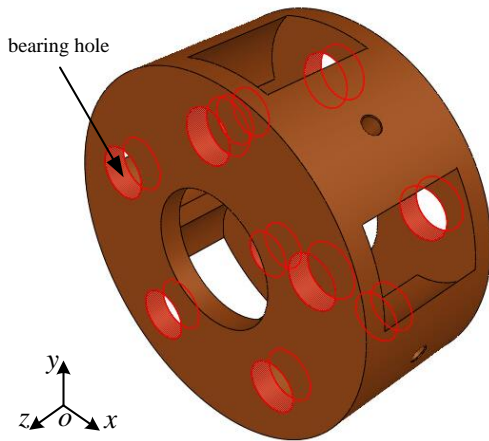


Fig.10 maximum displacement of bearing holes to be recorded as output response.

In order to be concise, *Mises* is used for representing von Mises stress of the frame, and *U<sub>max</sub>* denotes the displacement of the holes on the carrier. The mathematical expressions of the two responses are acquired by integrated DOE and RSM discussed in the following subsections.

### Python script program

In traditional design and analysis process shown in Fig.11 (a), three-dimensional model can be built in CAD software when values of all parameters are given. Then the model is usually imported into CAE software to finish engineering analysis for once. If analysis result cannot meet design requirements or size of the 3D model needs modifying, engineers need to do the process repeatedly, which wastes too much time for product development.

According to the optimization algorithm used in this paper, value of influential factor changes in each FEA, which causes the geometrical configuration changed at the same time. There are hundreds of times to invoke FEA for the optimization. Obviously, it is impractical to adopt traditional design process because superabundant manual intervention makes the optimization process time-consuming. Hence, building a parameterized simulation model applied in the process is of great significance and urgent need. To save time greatly, a fully automatic process shown in Fig.11 (b) is achieved during the optimization of the system.

Using python language and ABAQUS scripting interface (Hibbit et al., 2010), a program package for the parameterized model of the assembly is programmed on the re-development platform as embedded codes, which control FEA process automatically such as 3D component building, part assembling, loading, boundary condition defining, mesh generating, job submitting, response calculating and result postprocessing. The main function of the program is to achieve automation during FEA for preparation of DOE and RSM invoking.

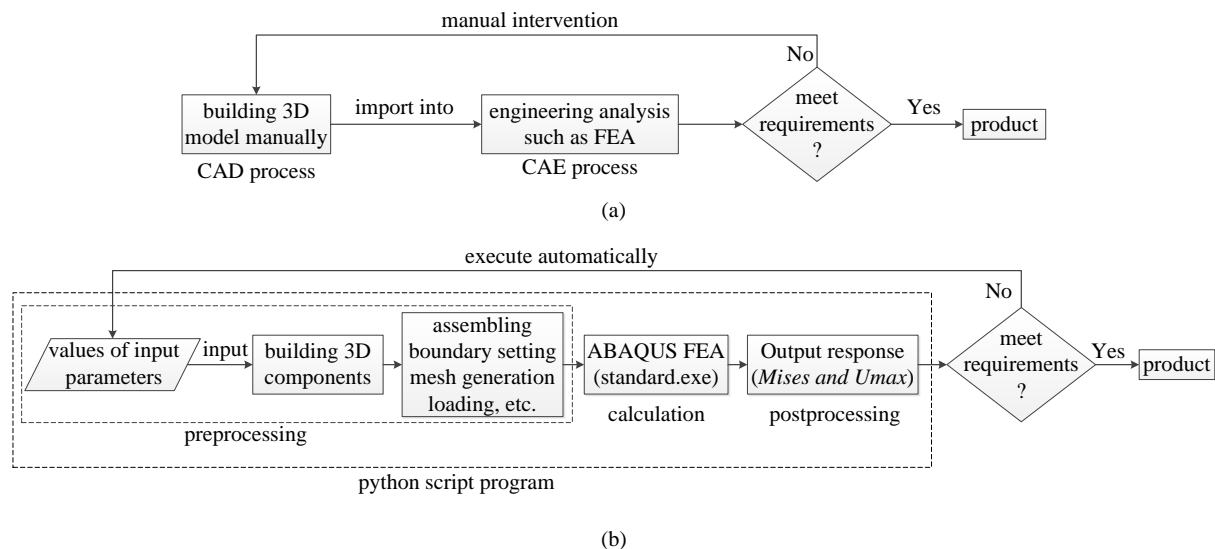


Fig.11 parameterized model simulation flow (b) compared with traditional design flow (a).

### Optimization flow

There are three main steps in the whole optimization process. First, via factorial design during DOE, significant factors are selected as design

variables for each of the two responses (*Mises* and *U<sub>max</sub>*). Second, RSM approximation models are established between the variables and each of the two responses through CCF design. Third,

through invoking the python script program, the optimization algorithm (LSGRG) will automatically finish the multi-objective optimal design. Thus, the Pareto efficient solution of the mathematic optimization model is obtained by the method.

Finally, the best geometrical configuration of the carrier assembled with the frame can be determined by integrated DOE, RSM and LSGRG.

The whole optimization flow is shown in Fig.12.

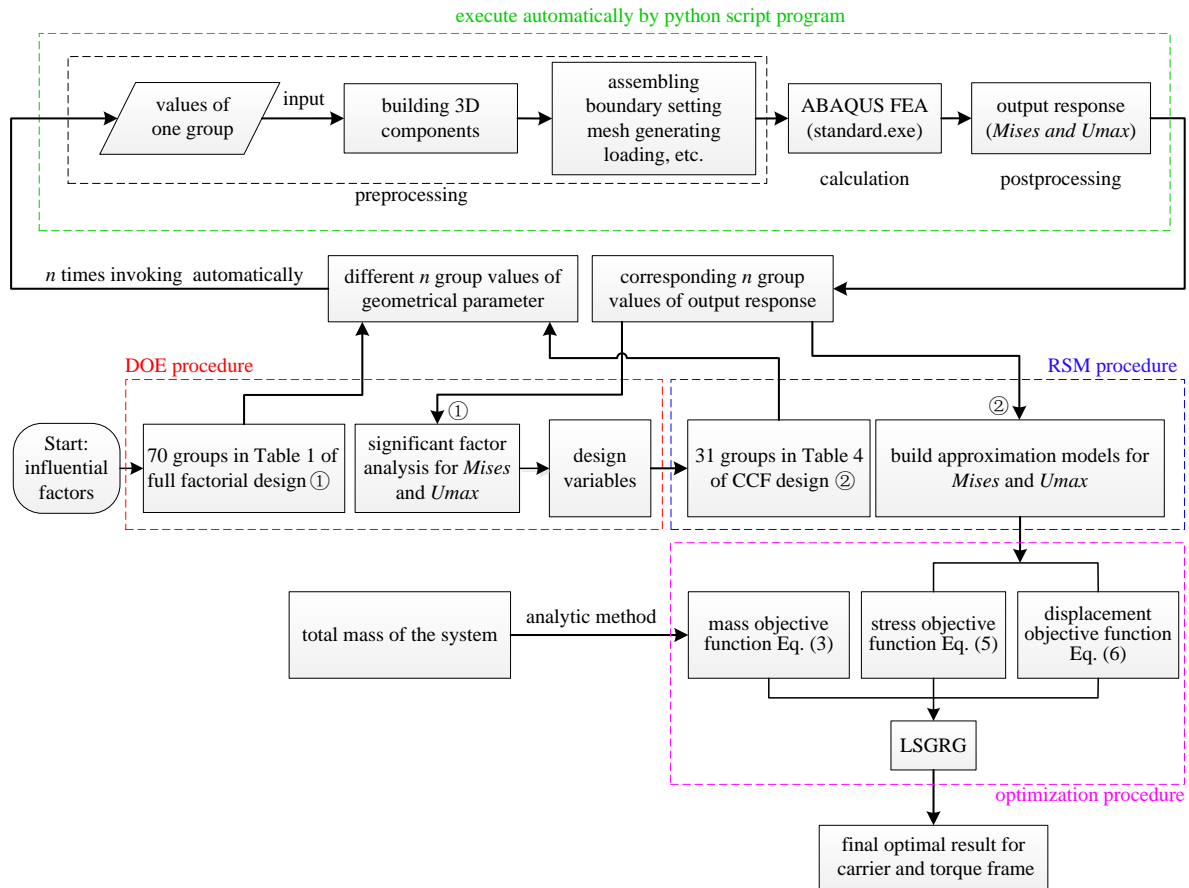


Fig.12 optimization flow for carrier and torque frame in GTF.

**DOE AND RSM**

To determine the explicit expressions of *Mises* and *Umax* effectively, DOE and RSM technologies are used as following description.

**Factorial design of DOE**

Full factorial design is used for the six influential factors to select the significant ones. There are totally 70 runs for the design, sixty-four of which are fundamental runs and six of which are central point runs. According to the basic dimension and assembly relationship among main components, value range of the six influential factors are finally determined as

$$\begin{cases} 1mm \leq V_1 \leq 9mm \\ 81^\circ \leq V_2 \leq 85^\circ \\ 195mm \leq V_3 \leq 205mm \\ 210mm \leq V_4 \leq 220mm \\ 1mm \leq V_5 \leq 7mm \\ 140mm \leq V_6 \leq 190mm \end{cases} \quad (4)$$

The DOE table of full factorial design including values of the two responses is shown in Table 1. The two responses are calculated by invoking python script program automatically.

Table 1 full factorial design for the six influential factors (including response value).

standard	run	coded						uncoded						responses	
		$V_1$	$V_2$	$V_3$	$V_4$	$V_5$	$V_6$	$V_1$ mm	$V_2$ degree	$V_3$ mm	$V_4$ mm	$V_5$ mm	$V_6$ mm	<i>Mises</i> MPa	<i>Umax</i> mm
45	1	-	-	+	+	+	-	1	81	205	220	7	140	84.62	0.06
28	2	+	+	-	+	-	+	9	85	195	220	1	190	43.30	0.06

C. Liu and Z.D. Fang: Multi-objective Optimal Design for Carrier and Torque Frame.

59	3	+	-	-	+	+	+	9	81	195	220	7	190	27.29	0.04
24	4	+	+	+	-	-	+	9	85	205	210	1	190	518.94	0.45
37	5	-	-	+	-	+	-	1	81	205	210	7	140	239.02	0.13
36	6	+	+	-	-	+	-	9	85	195	210	7	140	95.88	0.12
54	7	-	+	+	-	+	+	1	85	205	210	7	190	752.33	0.50
7	8	+	-	+	-	-	-	9	81	205	210	1	140	154.75	0.12
48	9	+	+	+	+	+	-	9	85	205	220	7	140	87.04	0.11
26	10	-	+	-	+	-	+	1	85	195	220	1	190	83.93	0.06
68	11	0	0	0	0	0	0	5	83	200	215	4	165	66.21	0.07
12	12	+	+	-	+	-	-	9	85	195	220	1	140	43.31	0.06
9	13	-	-	-	+	-	-	1	81	195	220	1	140	46.17	0.04
40	14	+	+	+	-	+	-	9	85	205	210	7	140	518.75	0.45
56	15	+	+	+	-	+	+	9	85	205	210	7	190	519.02	0.45
61	16	-	-	+	+	+	+	1	81	205	220	7	190	84.37	0.06
65	17	0	0	0	0	0	0	5	83	200	215	4	165	66.21	0.07
16	18	+	+	+	+	-	-	9	85	205	220	1	140	86.14	0.10
11	19	+	-	-	+	-	-	9	81	195	220	1	140	26.20	0.03
47	20	+	-	+	+	+	-	9	81	205	220	7	140	47.99	0.05
50	21	-	+	-	-	+	+	1	85	195	210	7	190	149.78	0.13
46	22	-	+	+	+	+	-	1	85	205	220	7	140	140.12	0.12
42	23	-	+	-	+	+	-	1	85	195	220	7	140	85.59	0.07
57	24	-	-	-	+	+	+	1	81	195	220	7	190	48.42	0.04
14	25	-	+	+	+	-	-	1	85	205	220	1	140	138.59	0.11
27	26	+	-	-	+	-	+	9	81	195	220	1	190	26.22	0.03
63	27	+	-	+	+	+	+	9	81	205	220	7	190	47.97	0.05
66	28	0	0	0	0	0	0	5	83	200	215	4	165	66.21	0.07
60	29	+	+	-	+	+	+	9	85	195	220	7	190	44.29	0.07
34	30	-	+	-	-	+	-	1	85	195	210	7	140	149.99	0.13
58	31	-	+	-	+	+	+	1	85	195	220	7	190	85.22	0.07
39	32	+	-	+	-	+	-	9	81	205	210	7	140	155.79	0.13
19	33	+	-	-	-	-	+	9	81	195	210	1	190	51.27	0.05
49	34	-	-	-	-	+	+	1	81	195	210	7	190	85.42	0.06
10	35	-	+	-	+	-	-	1	85	195	220	1	140	84.00	0.06
38	36	-	+	+	-	+	-	1	85	205	210	7	140	753.34	0.50
64	37	+	+	+	+	+	+	9	85	205	220	7	190	86.85	0.11
22	38	-	+	+	-	-	+	1	85	205	210	1	190	756.40	0.49
41	39	-	-	-	+	+	-	1	81	195	220	7	140	48.42	0.04
23	40	+	-	+	-	-	+	9	81	205	210	1	190	154.76	0.12
70	41	0	0	0	0	0	0	5	83	200	215	4	165	66.21	0.07
32	42	+	+	+	+	-	+	9	85	205	220	1	190	86.01	0.10
6	43	-	+	+	-	-	-	1	85	205	210	1	140	756.79	0.49
62	44	-	+	+	+	+	+	1	85	205	220	7	190	139.80	0.12
15	45	+	-	+	+	-	-	9	81	205	220	1	140	46.27	0.05
2	46	-	+	-	-	-	-	1	85	195	210	1	140	149.35	0.13
43	47	+	-	-	+	+	-	9	81	195	220	7	140	27.28	0.04
67	48	0	0	0	0	0	0	5	83	200	215	4	165	66.21	0.07
55	49	+	-	+	-	+	+	9	81	205	210	7	190	155.78	0.13
52	50	+	+	-	-	+	+	9	85	195	210	7	190	95.77	0.12
1	51	-	-	-	-	-	-	1	81	195	210	1	140	83.89	0.06
31	52	+	-	+	+	-	+	9	81	205	220	1	190	46.34	0.05
69	53	0	0	0	0	0	0	5	83	200	215	4	165	66.21	0.07
35	54	+	-	-	-	+	-	9	81	195	210	7	140	52.21	0.06
51	55	+	-	-	-	+	+	9	81	195	210	7	190	52.23	0.06
18	56	-	+	-	-	-	+	1	85	195	210	1	190	149.24	0.13
25	57	-	-	-	+	-	+	1	81	195	220	1	190	46.23	0.04
13	58	-	-	+	+	-	-	1	81	205	220	1	140	81.83	0.05
44	59	+	+	-	+	+	-	9	85	195	220	7	140	44.38	0.06
29	60	-	-	+	+	-	+	1	81	205	220	1	190	81.77	0.05
20	61	+	+	-	-	-	+	9	85	195	210	1	190	96.93	0.12
33	62	-	-	-	-	+	-	1	81	195	210	7	140	85.37	0.06
5	63	-	-	+	-	-	-	1	81	205	210	1	140	237.53	0.13
30	64	-	+	+	+	-	+	1	85	205	220	1	190	138.40	0.11
4	65	+	+	-	-	-	-	9	85	195	210	1	140	97.05	0.12
8	66	+	+	+	-	-	-	9	85	205	210	1	140	518.86	0.45
53	67	-	-	+	-	+	+	1	81	205	210	7	190	239.05	0.14
17	68	-	-	-	-	-	+	1	81	195	210	1	190	83.98	0.06
3	69	+	-	-	-	-	-	9	81	195	210	1	140	51.22	0.05
21	70	-	-	+	-	-	+	1	81	205	210	1	190	237.54	0.13

**Significant factors for *Mises* of torque frame**

Factorial effect to *Mises* response (standing for contribution to fitted model) is drawn in Fig.13 (a), from which the significant factors are selected from all influential factors. Particularly in significance test shown in Fig.13 (b), abscissa signifies t-value calculated in T-test.

Based on the given value of significance level  $\alpha$ , critical value of t-value is calculated. Usually  $\alpha$  is set as 0.05. On this occasion, factors whose absolute value is less than critical value are insignificant, whose absolute value is equal to or more than critical value are significant oppositely.

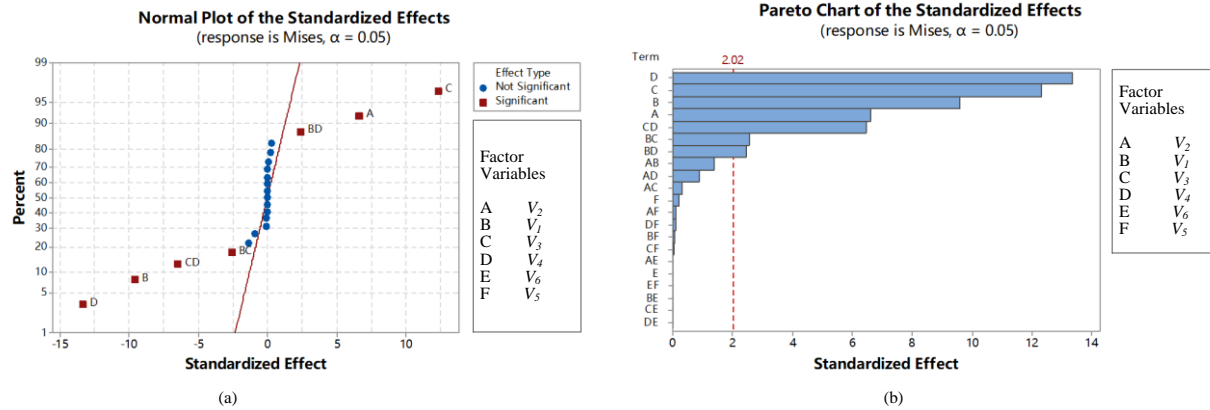


Fig.13 standardized effect plot of influential factors for *Mises* response.

To describe quantitative expression for the relationship between the four significant factors and *Mises*, its analysis of variance (ANOVA) is listed in Table 2. First, “P-value” indicates the effect of each polynomial term. In other words, it shows contribution to final expression. On the occasion where  $\alpha = 0.05$ , factors whose P-value is more than 0.05 are insignificant, whose P-value is equal to or less than 0.05 are significant, and especially whose P-value is equal to or less than 0.01 are extremely significant. Hence, one conclusion can be drawn from Table 2 that  $V_1, V_2, V_3$  and  $V_4$  are significant factors that make main contribution to *Mises*. This is reasonable because the four variables are all parameters belonging to torque frame qualitatively.

Second, “curvature” manifests whether the response surface is curve. P-value of curvature is equal to or less than 0.05 means quadratic polynomial regression is better than the linear. Third, “S” in model summary is square root of mean square of error. Apparently the closer to zero the value is, the more accurate the final expression is. Fourth, “R-sq.” and “R-sq. (adj)” are coefficients of determination for total model. Similarly, the closer to one the value is, the more accurate the final expression is. Besides, the closer the two values are, the better the total expression is. At last, “R-sq (pred)” reveals the difference between fitted expression and real value. Obviously, the expression is more accurate when “R-sq (pred)” is closer to one.

Table 2 ANOVA of significant factors for *Mises* in DOE.

Source		DF	Adj SS	Adj MS	F-Value	P-value
Model		7	162379	23197	82.36	0
	Linear	4	161534	40383.5	143.39	0
	$V_2$	1	19945	19945.4	70.82	0
	$V_1$	1	31977	31976.7	113.54	0
	$V_3$	1	73449	73449.5	260.79	0
	$V_4$	1	86396	86395.9	306.76	0
2-Way Interactions		3	22110	7370.1	26.17	0
	$V_1 * V_3$	1	1947	1947.2	6.91	0.011
	$V_1 * V_4$	1	1743	1743	6.19	0.016
	$V_3 * V_4$	1	18946	18946.2	67.27	0
Error		54	15209	281.6		
	curvature	1	11882	11881.6	189.28	0
Total		61	177588			
Model Summary	S	R-sq	R-sq(adj)	R-sq(pred)		
	16.7822	91.44%	90.33%	90.27%		

According to Table 2, P-value of the model including liner terms and 2-Way interaction terms are far less than 0.05. In addition, R-sq, R-sq. (adj) and R-sq. (pred) are all more than 90%. However, because P-value of curvature is close to zero and S

value is so large, linear model is not enough yet and quadratic polynomial model is needed. This conclusion is illustrated further in residual analysis shown in Fig.14 because the residual does not obey normal distribution in general.

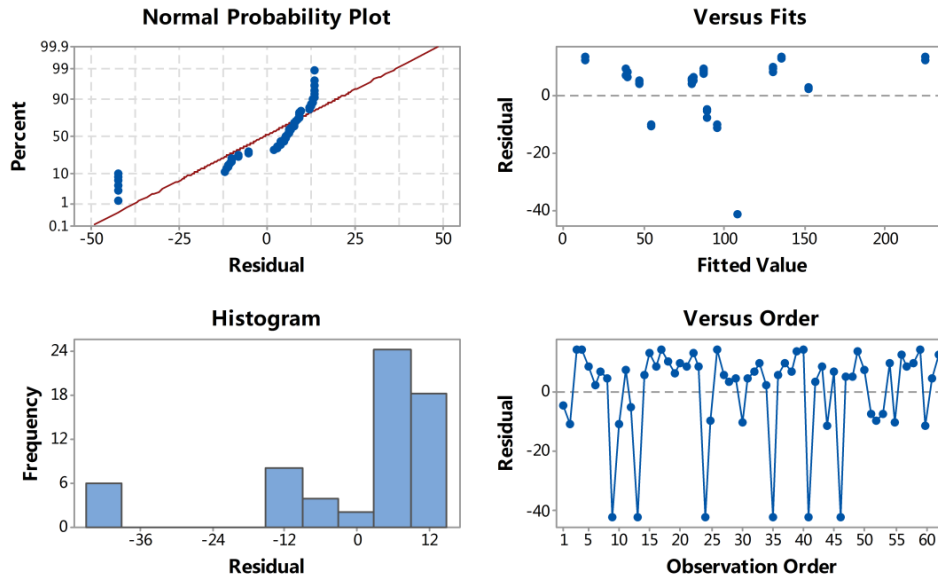


Fig.14 residual plots for *Mises* response in DOE.

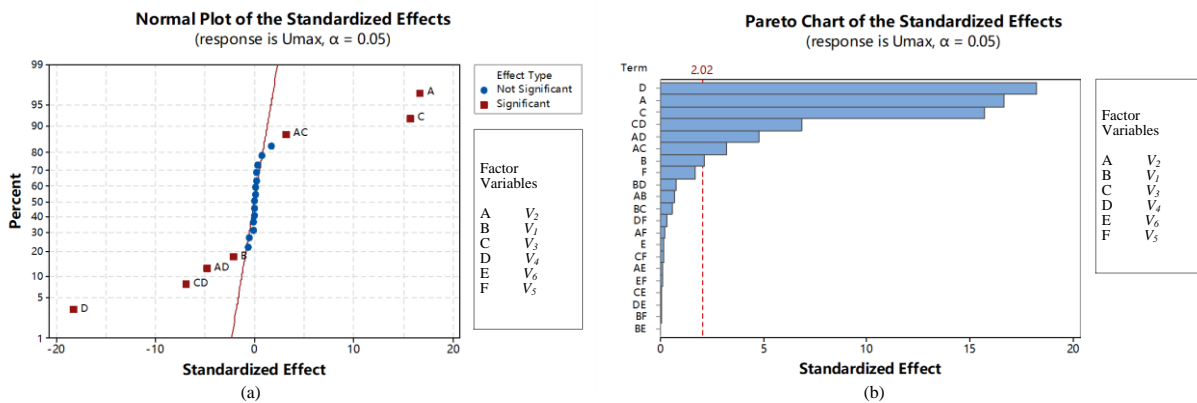


Fig.15 standardized effect plot of influential factors for *Umax* response

**Significant factors for *Umax* of holes on carrier**

Similarly, standardized effect of influential factors for *Umax* is shown in Fig.15, according to which that  $V_1$ ,  $V_2$ ,  $V_3$  and  $V_4$  are still significant factors for *Umax* when  $\alpha = 0.05$ . According to

corresponding ANOVA shown in Table 3, P-values of curvature is also close to zero, which means quadratic polynomial model is more appropriate than the linear. This conclusion is drawn according to residual analysis shown in Fig.16.

Table 3 ANOVA of significant factors for *Umax* in DOE.

Source	DF	Adj SS	Adj MS	F-Value	P-value
Model	7	0.066971	0.009567	111.73	0
Linear	4	0.046447	0.011612	135.61	0
$V_2$	1	0.028888	0.028888	337.37	0
$V_1$	1	0.00038	0.00038	4.43	0.04
$V_3$	1	0.025762	0.025762	300.86	0
$V_4$	1	0.03466	0.03466	404.77	0
2-Way Interactions	3	0.005242	0.001747	20.41	0
$V_2 * V_3$	1	0.001078	0.001078	12.59	0.001

		$V_2 * V_4$	1	0.002356	0.002356	27.51	0
		$V_3 * V_4$	1	0.004906	0.004906	57.3	0
Error		curvature	54	0.004624	0.000086		
Total			61	0.071595		466.66	0
Model	Summary	S	R-sq	R-sq(adj)	R-sq(pred)		
		0.0092536	93.54%	92.70%	92.73%		

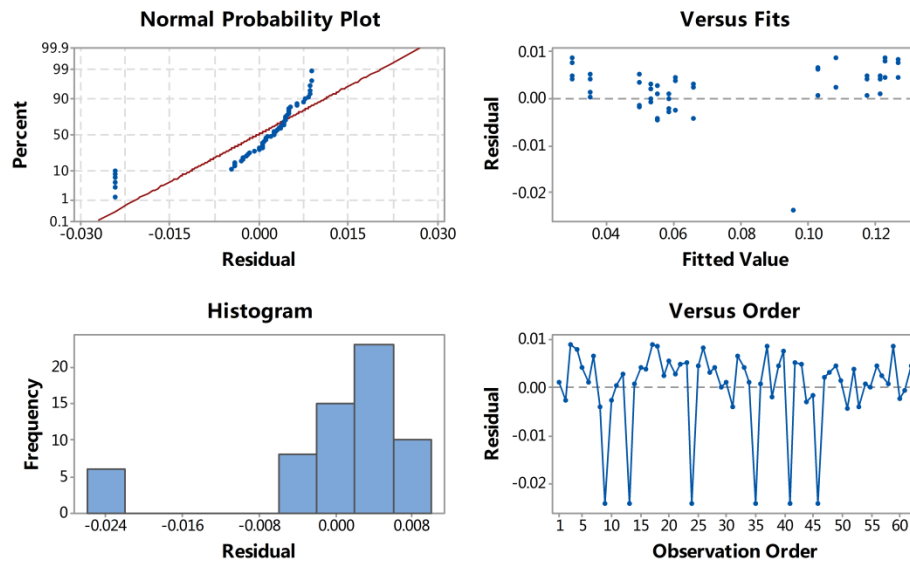


Fig. 16 residual plots for  $U_{max}$  response in DOE

**RSM approximation model**

Through DOE, there are four significant factors selected finally as design variables for  $Mises$  and  $U_{max}$ :  $V_1$ ,  $V_2$ ,  $V_3$  and  $V_4$ . However, both ANOVA and residual analysis prove that previous response surfaces of  $Mises$  and  $U_{max}$  are curve and linear polynomial is not suitable. Thus, a more accurate model needs building further. Consequently, the purpose of RSM next is to find a more suitable mathematical expression for the true functional relationship between input variables and responses. Usually, quadratic or high-order polynomial is chosen broadly. Certainly, it is unlikely that the expression is reasonable for the true functional relationship over the entire design space. However, it works quite well

for a relatively small region such as the range expressed in Equation(4). If the fitted response surface is adequate for the true relationship according to RSM, the model will be approximately equivalent to the actual function then.

Considering that value range of design point in Central Composite Design may exceed the range of input variable expressed in Eq.(4), Central Composite Face-centered design (CCF) is used to investigate the relationship between the four variables and the two responses respectively. The CCF design is shown in Table 4 including  $Mises$  and  $U_{max}$  response values, which are calculated by invoking python script program automatically as well.

Table 4 Central Composite Face-centered design (uncoded).

standard	run	$V_1$ mm	$V_2$ degree	$V_3$ mm	$V_4$ mm	$Mises$ MPa	$U_{max}$ mm
26	1	5	83	200	215	65.663	0.068792
4	2	9	85	195	210	97.02138	0.11798
2	3	1	85	195	210	149.1976	0.127105
27	4	5	83	200	215	65.663	0.068792
8	5	9	85	205	210	518.9098	0.450691
7	6	9	81	205	210	154.6776	0.12256
11	7	9	81	195	220	26.1167	0.034348
16	8	9	85	205	220	86.01048	0.103522
13	9	1	81	205	220	81.60687	0.050362
10	10	1	85	195	220	83.82019	0.061244

15	11	9	81	205	220	46.15571	0.047756
17	12	5	81	200	215	52.83577	0.051824
23	13	5	83	200	210	108.7317	0.105874
22	14	5	83	205	215	115.5398	0.098763
12	15	9	85	195	220	43.26227	0.0576
29	16	5	83	200	215	65.663	0.068792
20	17	9	83	200	215	63.4488	0.066598
28	18	5	83	200	215	65.663	0.068792
18	19	5	85	200	215	96.04564	0.114964
5	20	1	81	205	210	237.478	0.131308
1	21	1	81	195	210	83.87771	0.055983
24	22	5	83	200	220	46.08632	0.051759
31	23	5	83	200	215	65.663	0.068792
21	24	5	83	195	215	48.09409	0.054801
6	25	1	85	205	210	756.7305	0.494265
14	26	1	85	205	220	138.3391	0.110644
30	27	5	83	200	215	65.663	0.068792
25	28	5	83	200	215	65.663	0.068792
9	29	1	81	195	220	46.08633	0.036018
19	30	1	83	200	215	104.9956	0.070798
3	31	9	81	195	210	51.20717	0.052996

**Response surface model for *Mises***

The expression of the approximation model for *Mises* is written as

$$\begin{aligned}
 Mises = & 7193.32 + 58.027 \cdot V_2 + 30.2478 \cdot V_1 - 145.403 \\
 & \cdot V_3 + 42.1639 \cdot V_4 + 1.15921 \cdot V_1 \cdot V_1 + 0.6456 \\
 & \cdot V_3 \cdot V_3 + 0.226382 \cdot V_4 \cdot V_4 - 0.568605 \cdot V_2 \cdot V_1 \\
 & + 0.20707 \cdot V_2 \cdot V_3 - 0.389 \cdot V_2 \cdot V_4 - 0.57 \cdot V_3 \cdot V_4
 \end{aligned}
 \tag{5}$$

Its ANOVA is shown in Table 5. First, P-value of each term in the model is close to zero, which indicates that the fitted surface is effective and significant in general. Second, according to model summary, R-sq and R-sq(adj) (both over 99.95%) are exceedingly close with each other. This means the total model is much better than the linear. Third, R-sq (pred) value reaches up to 99.83% and S value is smaller relatively, which represents that the model is approximately equivalent to the actual function.

Table 5 ANOVA for *Mises* in RSM.

Source	DF	Adj SS	Adj MS	F-Value	P-value	
Model	11	18389.2	1671.74	5616.35	0	
Linear	4	14292.8	3573.2	12004.46	0	
	$V_2$	1	5393.5	5393.51	18119.93	0
	$V_1$	1	4587	4587.02	15410.48	0
	$V_3$	1	3774.1	3774.1	12679.41	0
	$V_4$	1	4049.6	4049.6	13604.97	0
Square	3	2458.1	819.36	2752.71	0	
	$V_1 * V_1$	1	661.1	661.07	2220.93	0
	$V_3 * V_3$	1	500.7	500.73	1682.24	0
	$V_4 * V_4$	1	57.8	57.79	194.15	0
2-Way Interaction	4	633.3	158.32	531.88	0	
	$V_2 * V_1$	1	166.6	166.57	559.6	0
	$V_2 * V_3$	1	20.2	20.18	67.79	0
	$V_2 * V_4$	1	71.2	71.18	239.13	0
	$V_3 * V_4$	1	484.8	484.82	1628.8	0
Total	21	18392.1				
Model Summary	S	R-sq	R-sq(adj)	R-sq(pred)		
	0.545579	99.98%	99.97%	99.83%		

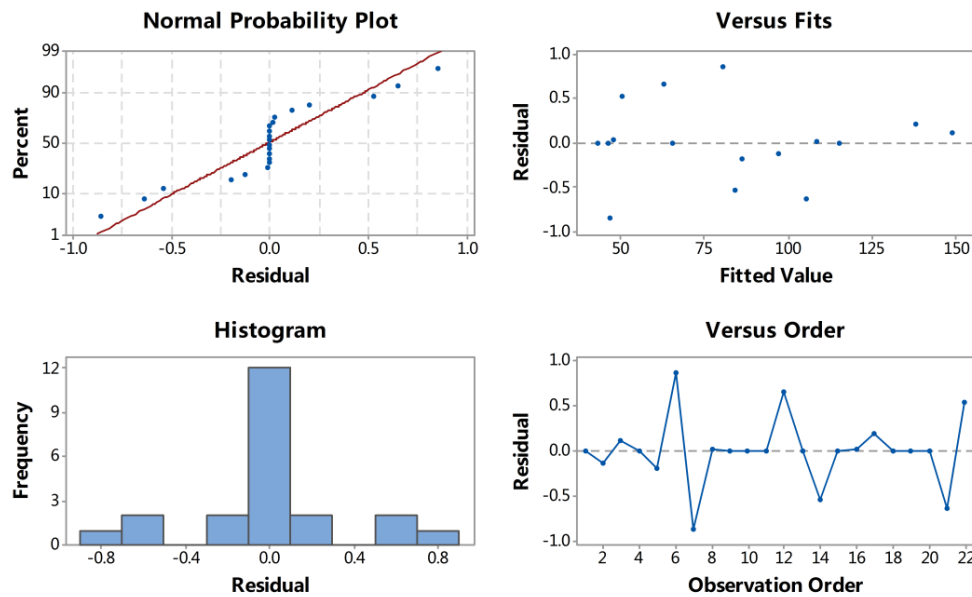


Fig.17 residual analysis for *Mises* in RSM.

In addition, the conclusions above are also certified by the residual analysis shown in Fig.17, in which the residuals obey Gaussian distribution generally. In sum, Eq.(5) is adequate to represent the relationship between the four variables and *Mises*.

**Response surface model for *Umax***

Similarly, the response surface model for *Umax* is obtained as

$$\begin{aligned}
 U_{max} = & 16.6866 - 0.50238 \cdot V_2 - 0.00062656 \cdot V_1 - 0.18 \cdot V_3 \\
 & + 0.201 \cdot V_4 + 0.00352246 \cdot V_2 \cdot V_2 + 0.0006 \cdot V_3 \cdot V_3 \\
 & + 0.00085 \cdot V_2 \cdot V_3 - 0.001 \cdot V_2 \cdot V_4 - 0.00058 \cdot V_3 \cdot V_4
 \end{aligned}
 \tag{6}$$

The corresponding ANOVA is listed in Table 6. First, P-values of all terms in the quadratic polynomial are close to zero, which indicates that the total model is significant generally. Second, according to model summary, R-sq and R-sq (adj) values (both over 99.50 %) are exceedingly close with each other. This means the model is effective further. Third, R-sq (pred) value reaches up to 99.30% and S value is much smaller relatively, which represents that the model is approximately equivalent to the actual function. In addition, these conclusions are also certified by the residual analysis shown in Fig.18, in which the residuals obey Gaussian distribution generally. In sum, Eq.(6) is available to represent the relationship between the four and *Umax*.

Table 6 ANOVA for *Umax* in RSM.

Source	DF	Adj SS	Adj MS	F-Value	P-value
Model	9	0.020808	0.002312	1201.04	0
Linear	4	0.014827	0.003707	1925.67	0
	$V_2$	0.009941	0.009941	5164.31	0
	$V_1$	0.000101	0.000101	52.22	0
	$V_3$	0.007713	0.007713	4007.08	0
	$V_4$	0.010466	0.010466	5437.03	0
Square	2	0.003725	0.001863	967.64	0
	$V_2 * V_2$	0.000501	0.000501	260.43	0
	$V_3 * V_3$	0.000518	0.000518	269.12	0
2-Way Interaction	3	0.001983	0.000661	343.34	0
	$V_2 * V_3$	0.000601	0.000601	312.46	0
	$V_2 * V_4$	0.001011	0.001011	525.36	0
	$V_3 * V_4$	0.001807	0.001807	938.55	0
Total	25	0.020838			
<b>Model Summary</b>					
	S	R-sq	R-sq(adj)	R-sq(pred)	
	0.0013874	99.85%	99.77%	99.30%	

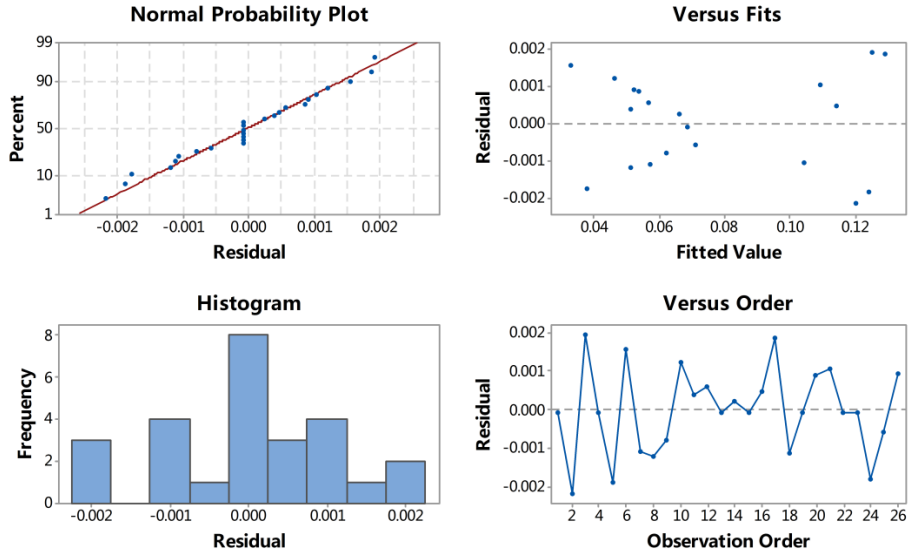


Fig.18 residual analysis for  $U_{max}$  in RSM.

### MULTI-OBJECTIVE OPTIMAL DESIGN AND MODEL VERIFICATION

The mathematic model of optimization for the carrier and frame of planetary gear train in GTF is expressed as

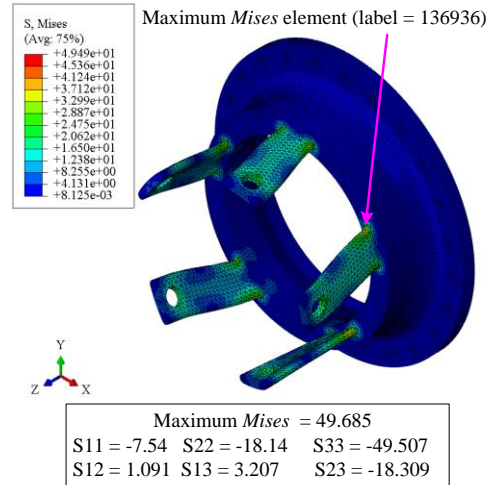
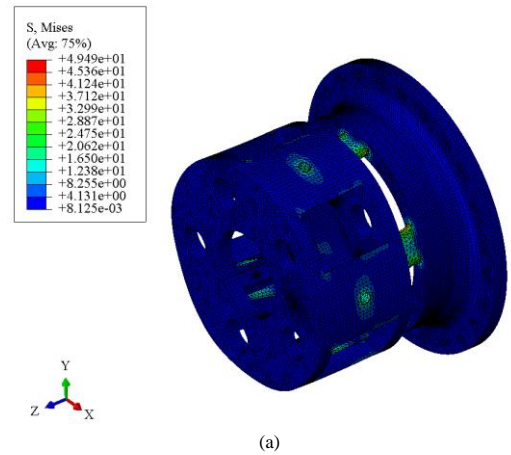
$$\begin{cases}
 \min M_{total} \\
 \min Mises \\
 \min U_{max} \\
 s.t. \quad 1 \leq V_1 \leq 9 \\
 \quad \quad 81 \leq V_2 \leq 85 \\
 \quad \quad 195 \leq V_3 \leq 205 \\
 \quad \quad 210 \leq V_4 \leq 220 \\
 \quad \quad 1 \leq V_5 \leq 7 \\
 \quad \quad 140 \leq V_6 \leq 190
 \end{cases} \quad (7)$$

Substituting Eq.(3), Eq.(5) and Eq.(6) into Eq.(7), the problem is solved by LSGRG method after normalization of each objective function, and the Pareto efficient solution is obtained as

$$\begin{cases}
 V_1 = 4.86 \text{ mm} \\
 V_2 = 81^\circ \\
 V_3 = 195 \text{ mm} \\
 V_4 = 210.23 \text{ mm} \\
 V_5 = 1 \text{ mm} \\
 V_6 = 140 \text{ mm}
 \end{cases} \quad (8)$$

To verify the mathematic optimization model, the Pareto efficient solution is substituted back into input variables in python script program to calculate

the responses again during FEA process. The FEA simulation results are shown in Fig.19 (gears are not shown). The total number of the nodes and elements are 104,240 and 497,537 respectively.



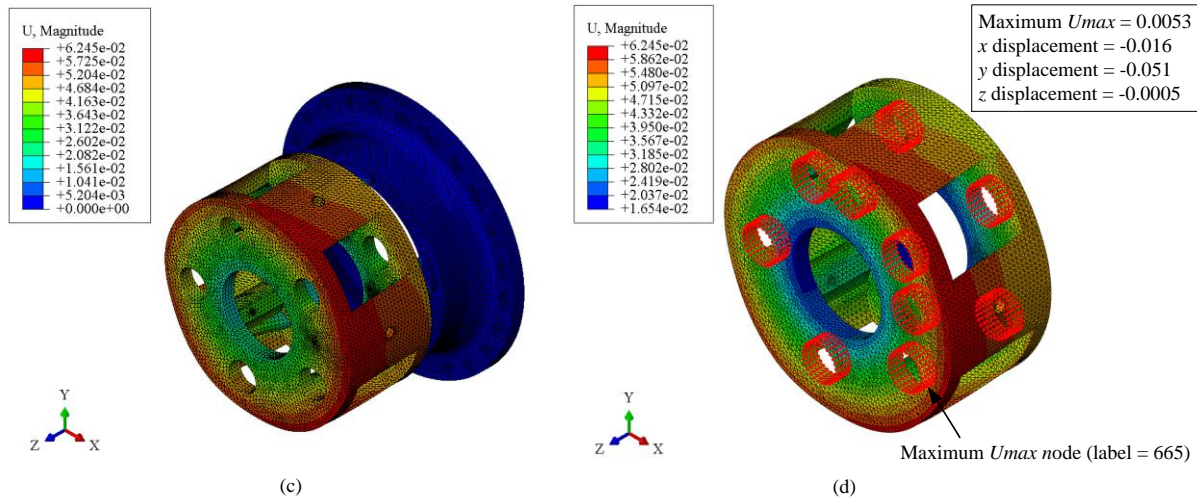


Fig.19 FEA results using the Pareto efficient solution as input variable values: (a) Mises nephogram of the assembly; (b) Mises nephogram of the frame; (c) Displacement nephogram of the assembly; (d) Displacement nephogram of the carrier.

The comparison of results by LSGRG and FEA is listed in Table 7, according to which the relative error of each response is less than 5%. This proves that the mathematic model expressed as Eq.(7) is quite correct firstly, and the Pareto efficient solution expressed as Eq.(8) can be used to determine the best configuration of the carrier and frame secondly. What's more, the method proposed in this paper also

displays advantage in CPU time. It took about 5.4 hours for 101 runs totally (including 70 DOE runs and 31 CCF-RSM runs) through invoking the python script program during FEA process, which indicates the method proposed is highly effective. Each analysis was run on a dual processor in a quad-core (Intel Xeon™ E5504 CPU, 2.0 GHz), 12.0 GB RAM personal computer.

Table 7 comparison of LSGRG and FEA results.

response	FEA(by ABAQUS)	LSGRG	Relative error (%)
<i>Umax</i> of holes on carrier	0.053 mm	0.054 mm	1.55
<i>Mises</i> of torque frame	49.685 MPa	48.142 MPa	3.11
Whole mass of the system	0.329 t	0.328 t	0.42

## CONCLUSIONS

A method of optimization design for carrier and torque frame assembled together in planetary gear train of GTF was proposed in this study. With ABAQUS scripting interface, a program package was coded as the parameterized model in Python language, which controls FEA process automatically for preparation of DOE and RSM invoking. The scripts include many functions such as assembling, loading, boundary condition defining, mesh generating, FE calculating and result extracting. To save computational resource greatly, proper treatments were performed to simplify the system. Multiple meshing strategies were applied with careful decision to guarantee high quality of grid during each FEA. Through DOE, significant factors were respectively selected as design variables for maximum von Mises stress of the frame and maximum displacement of the holes on the carrier. By CCF design, approximate quadratic polynomials were found as response

surface models to express the relationship between the four variables and the two responses respectively. The Pareto efficient solution of the mathematic optimization model was obtained by LSGRG algorithm for the three objectives (total mass, *Mises* and *Umax*).

FEA simulation results show that the model proposed is correct. The most favorable configuration of the assembly is determined by integrated DOE, RSM and LSGRG felicitously. This approach shows a wide application prospect especially in optimization problem of large-scale complicated system.

## ACKNOWLEDGMENT

The authors gratefully acknowledge the support of the National Natural Science Foundation of China (NSFC) through Grants Nos.51375384.

## REFERENCES

- Anderson-Cook, C. M., Borror, C. M., and Montgomery, D. C., “Response surface design evaluation and comparison”, *Journal of Statistical Planning and Inference*, Vol.139, pp. 629-641(2009).
- Ashjari, M., and Khoshrovan, M. R., “Mass optimization of functionally graded plate for mechanical loading in the presence of deflection and stress constraints”, *Composite Structures*, Vol.110, pp. 118-132(2014).
- Company Boeing, “Boeing Current Market Outlook 2015 to 2034”, Beijing, China, 2014.09.
- Fattahi, M., Kazemeini, M., Khorasheh, F., and Rashidi, A., “Kinetic modeling of oxidative dehydrogenation of propane (ODHP) over a vanadium–graphene catalyst: Application of the DOE and ANN methodologies”, *Journal of Industrial and Engineering Chemistry*, Vol.20, pp. 2236-2247(2014).
- Gurralla, P. K., and Regalla, S. P., “DOE Based Parametric Study of Volumetric Change of FDM Parts”, *Procedia Materials Science*, Vol.6, pp. 354-360(2014).
- Hansen, L. U., and Horst, P., “Multilevel optimization in aircraft structural design evaluation”, *Computers & Structures*, Vol.86, pp. 104-118(2008).
- Hibbit, Karlson, and Sorrenson, “ABAQUS user's manual (Version 6.10)”, Pawtucket, RI, USA, Dassault Systèmes Inc. 2010.
- Kuzmin, D., “An optimization-based approach to enforcing mass conservation in level set methods”, *Journal of Computational and Applied Mathematics*, Vol.258, pp. 78-86(2014).
- Losanno, D., Spizzuoco, M., and Serino, G., “An optimal design procedure for a simple frame equipped with elastic-deformable dissipative braces”, *Engineering Structures*, Vol.101, pp. 677-697(2015).
- Mccune, M. E., and Sheridan, W. G., *Method of assembly for gas turbine fan drive gear system in*, United Technologies Corporation (Hartford, CT, US) United States, 2014.
- Montgomery, D. C., *Design and analysis of experiments* (Eighth Edition), John Wiley & Sons Inc. Press, United States (2012).
- Relkar, A. S., and Nandurkar, K. N., “Optimizing & Analysing Overall Equipment Effectiveness (OEE) Through Design of Experiments (DOE)”, *Procedia Engineering*, Vol.38, pp. 2973-2980(2012).
- Sharma, N., Singh, A., Sharma, R., and Deepak, “Modelling the WEDM Process Parameters for Cryogenic Treated D-2 Tool Steel by Integrated RSM and GA”, *Procedia Engineering*, Vol.97, pp. 1609-1617(2014).
- Sheridan, W. G., *Fundamental gear system architecture in*, United Technologies Corporation (Hartford, CT, US) United States, 2013.
- Sheridan, W. G. S., *Epicyclic gear train for turbo fan engine in*, United Technologies Corporation (Hartford, CT, US) United States, 2012.
- Sheridan, W. G., *Fan drive gear system integrated carrier and torque frame in*, United Technologies Corporation (Hartford, CT, US) United States, 2014.
- Shin, M., Tortorelli, D. A., and Norato, J. A., “Optimal shape design of axisymmetric structures subject to asymmetric loading”, *Computer Methods in Applied Mechanics and Engineering*, Vol.293, pp. 283-305(2015).
- Si, Y., Karimi, H. R., and Gao, H., “Modelling and optimization of a passive structural control design for a spar-type floating wind turbine”, *Engineering Structures*, Vol.69, pp. 168-182 (2014).
- Wang, X., Chen, H., Liu, H., Li, P., Yan, Z., Huang, C., Zhao, Z., and Gu, Y., “Simulation and optimization of continuous laser transmission welding between PET and titanium through FEM, RSM, GA and experiments”, *Optics and Lasers in Engineering*, Vol.51, pp. 1245-1254(2013).
- Zhan, W., Cui, Y., Feng, Z., Cheung, K. C., Lam, J., and Gao, H., “Joint optimization approach to building vibration control via multiple active tuned mass dampers”, *Mechatronics*, Vol.23, pp. 355-368(2013).
- Zhou, M., and Wang, M. Y., “Engineering feature design for level set based structural optimization”, *Computer-Aided Design*, Vol.45, pp. 1524-1537(2013).

## APPENDIX

I. According to values of basic geometrical and physical parameters of the system, mass of the carrier, torque frame and gears are determined respectively as

$$M_{carrier} = M_{10} - M_{aper} = 0.1014 - 5 \cdot \rho \cdot V_6 \cdot \left[ \pi \cdot r_2^2 + \frac{\pi \cdot R_4^2}{360} \cdot (180 - 2\alpha) - \frac{\pi \cdot R_3^2}{360} \cdot (180 - 2\alpha) \right]$$

$$M_{torframe} = M_{20} + M_{finger} = 0.0846 + 5 \cdot \rho \cdot 190 \cdot \left[ \pi \cdot r_1^2 + \frac{\pi \cdot R_2^2}{360} \cdot (180 - 2\alpha) - \frac{\pi \cdot R_1^2}{360} \cdot (180 - 2\alpha) \right]$$

$$M_{gears} = M_{sun} + M_{star} + M_{ring}$$

## NOMENCLATURE

$V_1$	fillet radius of the finger
$V_2$	finger angle
$V_3$	inner radius of finger
$V_4$	outer radius of finger
$V_5$	clearance between the finger and aperture when assembled together
$V_6$	depth of the carrier aperture receiving the finger
$\rho$	material density
$M_{total}$	total mass of the system
$M_{carrier}$	mass of the carrier
$M_{aper}$	mass of apertures on the carrier
$M_{torframe}$	mass of the torque frame
$M_{finger}$	mass of the fingers on the frame
$M_{gears}$	mass of all gears
$M_{sun}$	mass of sun gear
$M_{star}$	mass of star gears (intermediate gears)
$M_{ring}$	mass of ring gear

## 基于集成 DOE, RSM 和 LSGRG 方法的 GTF 行星架 與力矩器多目標優化設計

劉超 方宗德  
西北工業大學機電學院

### 摘要

本文針對齒輪驅動渦扇發動機 (GTF) 星型輪系中行星架與力矩器的裝配體結構提出了一種多目標優化設計方法。首先, 採用 Python 語言編制了該系統參數化模型的程序包。該程序的主要作用是實現整個優化過程中對全有限元分析過程的自動化調用, 從而極大地縮短了產品的研發周期。其次, 通過試驗設計方法 (DOE) 分別確定了力矩器最大馮米塞斯應力及行星架軸孔處最大位移的顯著因子。再次, 通過中心複合表面設計 (CCF) 獲得了這兩個響應變量的採樣值。然後利用響應面 (RSM) 方法建立了近似的二次多項式以表達這兩個目標函數的顯式關係式。最後, 使用大規模廣義簡約梯度法 (LSGRG) 求解了該優化問題的 Pareto 有效解。仿真結果的驗證表明, 三個優化變量 (總質量、最大馮米塞斯應力及最大位移) 的相對誤差均不超過 5%, 這說明本文所提出的模型是正確的。結果對比還表明, 為了確定該裝配體的最佳構型, 綜合的 DOE、RSM 及 LSGRG 方法是恰當且高效的。